BALANCING SAFETY AND RETURN: REGION-BASED REWARD PENALTY OVER ACTION CHUNKS FOR OFFLINE SAFE RL

Anonymous authors
Paper under double-blind review

ABSTRACT

In-sample learning has emerged as a powerful paradigm that mitigates the Out-of-Distribution (OOD) issue, which leads to violations of safety constraints in offline safe reinforcement learning (OSRL). Existing approaches separately train reward and cost value functions, yielding *suboptimal* policies within the safe policy space. To address this, we propose the *Region-Based Reward Penalty over Action Chunks* (R2PAC), a novel method that trains h-step optimal value function within the safe policy space. By penalizing reward signals over action chunks that may potentially lead to unsafe transitions, our method: (1) integrates cost constraints into reward learning for constrained return maximization; (2) improves joint training stability by accelerating the convergence speed with unbiased multi-step value estimation; (3) effectively avoids unsafe states through temporally consistent behaviors. Extensive experiments on the DSRL benchmark demonstrate that our method outperforms state-of-the-art algorithms, achieving the highest returns in 13 out of 17 tasks while maintaining the normalized cost below a strict threshold in all tasks. The proposed method can be used as a drop-in replacement within existing offline RL pipelines.

1 INTRODUCTION

Despite the potential to mitigate online safety risks, OSRL still inherits fundamental challenges from both safety guarantees and offline regularization. A major challenge in offline reinforcement learning (RL) is distributional shift (Levine et al., 2020; Fujimoto et al., 2019), wherein unseen state-action pairs are often erroneously overestimated to have unrealistic values (Fujimoto et al., 2019). This overestimation makes the policy preferentially select OOD actions during deployment. To address these challenges, existing offline RL works propose to constrain the learned policy close to the behavior policy or penalize the Q-values of OOD actions (Fujimoto et al., 2019; Kumar et al., 2020; An et al., 2021; Kumar et al., 2019; Fujimoto and Gu, 2021). However, such approaches may result in overly conservative policies (Mao et al., 2023). Another class of methods, in-sample learning (Kostrikov et al., 2021; Hansen-Estruch et al., 2023; Xu et al., 2023; Garg et al., 2023; Xiao et al., 2023) such as implicit Q-learning (IQL) (Kostrikov et al., 2021), offers a potential alternative that effectively avoids the OOD issue. In-sample learning approximates optimal values without querying the value function of any unseen actions. In addition, its decoupled value function and policy learning processes provide additional feasibility to various parameterized actors (Hansen-Estruch et al., 2023; Zheng et al., 2024; Wang et al., 2023).

A major challenge imposed by safety constraints is the necessity of preventing unsafe actions that could result in catastrophic outcomes (García et al., 2015; Ray et al., 2019; Brunke et al., 2022; Andersen et al., 2020; Shi et al., 2021). A magnitude of safe RL approaches, such as primal-dual methods (Wu et al., 2024; Chow et al., 2018) and reward penalty techniques (Thomas et al., 2021; Araújo and Braga, 1998), fail to consistently satisfy constraints despite their foundation in constrained optimization, resulting in significant training performance instability. Feasibility analysis (Fisac et al., 2019; Yu et al., 2022) can effectively enforce constraints, though its strong focus on constraint satisfaction may result in overly conservative policies.

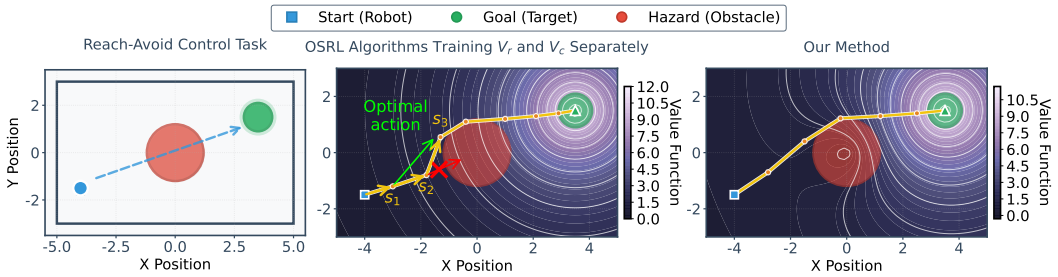

Figure 1: An illustrative example of a reach-avoid control task. Left: The robot aims to reach the goal while avoiding hazards. Middle: Under decoupled value functions, the robot at s_1 myopically chooses the action maximizing V_r (yellow arrow to s_2). At s_2, the V_r-maximizing action is unsafe (red arrow), forcing a safe alternative (yellow arrow to s_3) by V_c. However, the globally optimal trajectory requires selecting the green arrow at s_1. Right: In contrast, incorporating a reward penalty into IQL encourages a coherent value function that balances safety and task achievement, resulting in a shorter and more efficient hazard avoidance path toward the goal.

While the offline in-sample method IQL shows potential for incorporating safety constraints (Koirala et al., 2025; Zheng et al., 2024), it faces significant challenges in guaranteeing safety. In the existing research, the independent training of reward and cost value functions can lead to the extracted policy diverging from the optimal policies implied by each value function, thereby risking safety failures or performance degradation. As shown in Figure 1, the separate training of reward and cost value functions leads them to provide conflicting policy recommendations, forcing the policy onto a suboptimal trajectory. In contrast, jointly training the value functions enables the agent to foresee potential risks while pursuing reward maximization.

To address this issue, different from existing in-sample OSRL methods with separate training of the reward and cost value function, we propose the *Region-Based Reward Penalty over Action Chunks* (R2PAC), a novel in-sample OSRL method that is the first approach to enable IQL to directly learn a single value function whose corresponding implicit policy is optimal within the safe policy space. Our method introduces two effective extensions to the IQL algorithm, achieving strong performance in both reward maximizing and constraint satisfaction.

The first innovation is on a new region-based reward-penalized update within the IQL framework, which extends the reward value function of IQL to incorporate safety constraints. The key breakthrough is that a straightforward yet powerful region-specific reward penalty enables the standard IQL framework to learn a value function that corresponds to the constrained optimal policy. Specifically, a key step is to learn an optimal cost value function, through which we accurately identify safe regions and establish a well-defined region that guides our targeted penalty design. Subsequently, we penalize the reward signal for transitions into unsafe areas. Theoretical analysis shows that this penalization ensures policy safety without sacrificing optimality, which is supported by our argument that an unsafe policy is always inferior to a safe one under our penalization. As a result, safe policy extraction can be simplified using only a single value function.

We propose, for the first time, integrating action chunking, a technique widely employed in imitation learning (Black et al., 2025; Li et al., 2025), into in-sample learning to stabilize the training of value functions and to enhance its risk anticipation capability. First, we identify for the first time that, by leveraging multi-step backpropagation to mitigate the impact of temporal difference (TD) errors, action chunking helps to address the overfitting problem, a common issue in in-sample learning methods (Chen et al., 2025; Xu et al., 2023; Garg et al., 2023). Furthermore, since our reward value function is trained in dependency on the cost value function, action chunking helps stabilize the training of the reward value function compared to single-step updates. Secondly, by predicting action sequences over the next h steps, our method significantly improves the agent's danger avoidance capability. In contrast to single-step prediction, our approach equips the actor with implicit long-horizon foresight, enabling earlier anticipation of potential hazards.

The proposed method is straightforward to implement and highly transferable to most OSRL algorithms, as it requires no additional modules and uses a simple multi-layer perceptron (MLP) as the

network backbone. Indeed, merely by changing to rely on a single value function and incorporating action chunking, we can avoid the challenge faced by existing in-sample learning methods in balancing the contributions of reward and cost value functions.

Extensive experimental results demonstrate that our method outperforms other OSRL algorithms on the DSRL benchmark (Liu et al., 2023a). Adopting only a single value function for policy extraction, our method satisfies safety constraints across all 17 tasks and achieves the highest reward in 13 of them.

2 Related Work

Offline Safe RL. Safe offline RL learns policies from fixed datasets under safety constraints, commonly formulated as a Constrained Markov Decision Process (CMDP) (Altman, 2021). Existing methods often combine Lagrangian-based safe RL techniques with offline algorithms (Kostrikov et al., 2021; Xu et al., 2022; Zheng et al., 2024). Representative works include CPQ (Xu et al., 2022), which penalizes unsafe and OOD actions but may harm generalization, and FISOR (Zheng et al., 2024), which enforces strict safety via Hamilton–Jacobi reachability. Alternative sequence modeling approaches (Liu et al., 2023b; Lin et al., 2023; Zhang et al., 2023) exist but are sensitive to data quality.

Action Chunking. Action chunking has been widely used in imitation learning to improve policy robustness and handle non-Markovian behavior in offline datasets (Li et al., 2025; Black et al., 2025; Liu et al., 2025; Bharadhwaj et al., 2024; George and Farimani, 2023). This approach predicts and executes action sequences in an open-loop manner, requiring a powerful parameterized actor. Learning such chunked policies often relies on expressive generative models, including diffusion (Sohl-Dickstein et al., 2015; Ho et al., 2020; Song et al., 2020; Croitoru et al., 2023) and flow matching (Frans et al., 2025; Gao et al., 2025; Lipman et al., 2024; Chen and Lipman, 2023; Lipman et al., 2022). In this work, we repurpose action chunking to regularize the value function and promote safety through temporally consistent actions in in-sample learning.

3 Preliminary

Offline Safe RL. Safe RL is typically formulated as a CMDP (Altman, 2021), which is defined by a tuple $\mathcal{M} := (\mathcal{S}, \mathcal{A}, P, r, c, \gamma)$. This tuple comprises a state space $\mathcal{S}$, an action space $\mathcal{A}$, a transition dynamics $P : \mathcal{S} \times \mathcal{A} \to \Delta(\mathcal{S})$, a reward function $r : \mathcal{S} \times \mathcal{A} \to \mathbb{R}$, a cost function $c : \mathcal{S} \times \mathcal{A} \to \mathbb{R}$, and a discount factor $\gamma \in [0, 1]$. The objective of safe RL is to find a policy $\pi(a|s)$ to maximize the expected cumulative rewards while satisfying the safety constraint, i.e. $\max_\pi \mathbb{E}_{s_0\sim\rho_0, a_t\sim\pi, s_{t+1}\sim P}\big[\sum_{t=0}^{T-1}\gamma^t r(s_t, a_t)\big],\ s.t. \mathbb{E}_{s_0\sim\rho_0, a_t\sim\pi, s_{t+1}\sim P}\big[\sum_{t=0}^{T-1}\gamma^t c(s_t, a_t)\big] \le \ell$, where ρ_0 denotes the distribution of initial states, T is the trajectory length, and $\ell \ge 0$ is the predefined cost limit.

In offline RL, the objective is to optimize the safe RL objective with a previously collected dataset $\mathcal{D} = \{(s_t^{(i)}, a_t^{(i)}, r_t^{(i)}, c_t^{(i)}, s_{t+1}^{(i)})_{t=0}^{T-1}\}_{i=0}^{N-1}$, which contains a total of N trajectories. Existing offline safe RL methods typically solve the problem in the following form:

$$\max_\pi \quad \mathbb{E}_{s_t,a_t}\left[\sum_{t=0}^{T-1}\gamma^t r(s_t, a_t)\right] \quad \text{s.t.} \quad \mathbb{E}_{s_t,a_t}\left[\sum_{t=0}^{T-1}\gamma^t c(s_t, a_t)\right] \le \ell; \quad D(\pi||\pi_\beta) \le \epsilon, \tag{1}$$

where π_β is the underlying behavioral policy of the offline dataset, $D(\pi||\pi_\beta)$ is a divergence term to prevent the learned policy π shift form π_β.

Implicit Q Learning. IQL (Kostrikov et al., 2021) addresses the distribution shift issue by approximating value functions only on in-distribution data. This method is achieved through an asymmetric ℓ_2 loss (i.e., expectile regression). The losses for parameterized Q-function and state value function in IQL are as follows:

$$\mathcal{L}_Q(\theta) = \mathbb{E}_{(s,a,s')\sim D}\left[\left(r(s, a) + \gamma V_\psi(s') - Q_\theta(s, a)\right)^2\right], \tag{2}$$

$$\mathcal{L}_V(\psi) = \mathbb{E}_{(s,a)\sim D}\left[L_2^\tau(Q_{\hat{\theta}}(s, a) - V_\psi(s))\right], \tag{3}$$

where $L_2^\tau(u) = |\tau - \mathbb{I}(u < 0)|u^2$. For policy extraction, IQL uses Advantage Weighted Regression (AWR) (Peng et al., 2019):

$$\mathcal{L}_\pi(\phi) = \mathbb{E}_{(s,a)\sim D}\left[\exp(\alpha(Q_{\hat{\theta}}(s,a) - V_\psi(s)))\log \pi_\phi(a|s)\right], \tag{4}$$

where $\alpha \in [0, \infty]$ is the temperature parameter.

4 METHODS

In this section, we introduce the formulation of the proposed *region-based reward penalty over action chunks*, which yields a single value function to achieve both reward maximization and constraint satisfaction. Our approach comprises three key components: (1) the derivation of a region-based reward penalty mechanism, (2) the adaptation of action chunking to stabilize value function training, and (3) a simple yet effective policy extraction method based on flow-matching.

4.1 PENALIZED REWARD VALUE FUNCTION

To address safety requirements in offline RL, we first introduce a penalized value function. Our objective is to learn a policy that consistently satisfies safety constraints, relying solely on in-sample data.

We first separate the entire state space $\mathcal{S}$ into the *safe region* ($\mathcal{S}^\pi_{\text{safe}}$) and the *unsafe region* ($\mathcal{S}^\pi_{\text{unsafe}}$). Following the conventions established in prior work (Fisac et al., 2019; Zheng et al., 2024; Thomas et al., 2021), we have the following definition:

Definition 1 *The safe region and the unsafe region under a policy π are defined as:*

$$\mathcal{S}^\pi_{safe} \coloneqq \{s \in \mathcal{S} | V_c^\pi \leq \ell\} \quad \textit{and} \quad \mathcal{S}^\pi_{unsafe} \coloneqq \mathcal{S}/\mathcal{S}^\pi_{safe}. \tag{5}$$

We denote $\mathcal{S}^*_{\text{safe}}$ as the largest safe region, which is induced by the policy $\pi_c^* \coloneqq \arg\min_{\pi\in\Pi} V_c^\pi(s)$. By definition, for any state within $\mathcal{S}^*_{\text{safe}}$, there exists at least one policy that satisfies the safety constraints from that state onward. Conversely, if a state belongs to $s \in \mathcal{S}^*_{\text{unsafe}} \coloneqq \mathcal{S}/\mathcal{S}^*_{\text{safe}}$, any trajectory starting from it will eventually violate the safety threshold ℓ, since even the safest feasible policy π_c^* fails to satisfy the constraint at s. Accordingly, we define the safe policy space as follows:

Definition 2 *The safe policy space is defined as:*

$$\Pi_{safe} \coloneqq \{\pi \in \Pi | V_c^\pi(\rho_0) \leq \ell\}, \tag{6}$$

where ρ_0 is the initial state distribution.

Region-Based Reward Penalty Framework. Inspired by Thomas et al. (2021), we adopt the reward penalty framework to ensure safety. For a transition (s, a, s', r), we transform it to:

$$(s, a, s', r) = \begin{cases} (s, a, s', r) & \text{If } s' \in \mathcal{S}^*_{\text{safe}} \\ (s, a, s_a, -C) & \text{If } s' \in \mathcal{S}^*_{\text{unsafe}} \end{cases}, \tag{7}$$

where $C \in \mathbb{R}$ is a penalty constant for unsafe transitions, and s_a denotes an absorbing state: any action taken in s_a returns to s_a with reward $-C$. Under this formulation, any unsafe action that would lead to an unsafe next state is effectively redirected to s_a. Intuitively, provided that C is sufficiently large, any policy that maximizes cumulative reward from a safe state s is guaranteed to avoid entering the unsafe region. We denote the reward value function learned with this transformation as $\overline{V}_r$. To formalize this intuition, we present the following proposition:

Proposition 1 *Assume that the safe policy space Π_{safe} is non-empty for any $\ell \geq 0$. Then for any safe policy $\pi_1 \in \Pi_{safe}$ and any unsafe space $\pi_2 \in \Pi/\Pi_{safe}$, the value functions satisfy*

$$\overline{V}_r^{\pi_1}(\rho_0) > \overline{V}_r^{\pi_2}(\rho_0) \tag{8}$$

under the condition

$$C > \frac{\sum_{t=0}^{T-1}\gamma^t(r_{\max} - r_{\min})}{\ell}, \tag{9}$$

where $r_{\max}$ and $r_{\min}$ denote maximum and minimum of the reward.

The above discussion ensures that, starting from a safe state, a policy maximizing $\overline{V}_r$ will, in theory, never enter the unsafe region. Moreover, we demonstrate that our penalty framework also preserves optimality when extended to hard constraints. The proof and corresponding discussion are provided in Appendix A.1 and Appendix A.2.

Learning the Safe and Reward Value Functions. We employ IQL to learn the optimal cost value functions Q_c^*, V_c^* using

$$\mathcal{L}_{Q_c} = \mathbb{E}_{(s,a,s')\sim D}\Big[(c(s,a) + \gamma V_c(s') - Q_c(s,a))^2\Big], \tag{10}$$

$$\mathcal{L}_{V_c} = \mathbb{E}_{(s,a)\sim D}\Big[L_2^\tau(V_c(s,a) - Q_c(s))\Big], \tag{11}$$

Based on V_c^*, we derive the largest safe region $\mathcal{S}^*_{\text{unsafe}}$. Additionally, we apply the same IQL framework to learn the optimal reward value function using the converted transition data:

$$\mathcal{L}_{\overline{Q}_r} = \mathbb{E}_{(s,a,s')\sim D}\Big[(\mathbb{I}(V_c(s') \le \ell)(r(s,a) + \gamma\overline{V}_r(s')) + \mathbb{I}(V_c(s') > \ell)\overline{C} - \overline{Q}_r(s,a))^2\Big], \tag{12}$$

$$\mathcal{L}_{\overline{V}_r} = \mathbb{E}_{(s,a)\sim D}\Big[L_2^\tau(\overline{Q}_r(s,a) - \overline{V}_r(s))\Big], \tag{13}$$

where $\overline{C} = \frac{-C}{1-\gamma} = \sum_{t=0}^{\infty}\gamma^t(-C)$ denotes the value of the absorbing state s_a, and $\mathbb{I}(\cdot)$ represents the indicator function. To extract a policy that maximizes cumulative reward while satisfying safety constraints, it suffices to maximize the penalized reward value function $\overline{V}_r$.

4.2 Penalized Value Function with Action Chunking

Although Section 4.1 offers a theoretically justified framework for safety guarantees, the training of the penalized reward value function $\overline{V}_r$ can exhibit instability caused by the dependency of $\overline{V}_r$ on V_c, where bootstrap errors propagate across both temporal horizon and value functions. To address this, we integrate an action chunking technique into the IQL framework for value function learning.

Chunked Q-function. We generalize the critic training to operate over a horizon of h consecutive actions:

$$Q_r(s_t, a_{t:t+h}) = \sum_{k=t}^{t+h-1}\gamma^k r_k + \gamma^h V_r(s_{t+h}), \quad Q_c(s_t, a_{t:t+h}) = \sum_{k=t}^{t+h-1}\gamma^k c_k + \gamma^h V_c(s_{t+h}), \tag{14}$$

where $a_{t:t+h} = \{a_t, a_{t+1}, \cdots, a_{t+h-1}\}$.

The chunked Q-function described above exhibits a structural similarity to the uncorrected n-step return (Kozuno et al., 2021; Hessel et al., 2018), which introduces bias by conditioning only on the first action while using rewards from a sequence of actions. In contrast, our method remains unbiased, as the Q-function explicitly takes the entire action sequence as input.

Alleviate Overfitting in IQL. In IQL, the use of a large τ (close to 1) in the asymmetric loss function leads to better approximate the maximum value function. However, this approach can cause the value function to overfit to overestimated Q-values originating from bootstrap errors. We present the first analysis of Q-value overestimation in IQL from a temporal horizon perspective, and introduce an action chunking technique to mitigate the effect of bootstrap errors. The overestimation is primarily due to the propagation of bootstrap errors during the standard 1-step temporal difference backups. This propagation results in cumulative error amplification over extended temporal horizons.

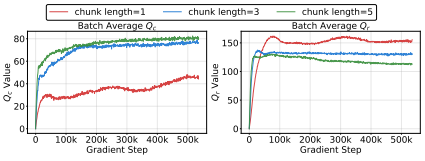

Figure 2: Batch-averaged Q_r and Q_c values obtained during training with vanilla IQL on the Bullet-Safety-Gym *BallRun* task across various chunk lengths.

Unlike previous studies that mitigate overfitting via value ensembles in 1-step IQL (Chen et al., 2025), our action chunking technique reduces approximation error and enhances numerical stability by decreasing error propagation frequency without a huge number of value networks. The use of h-step returns propagates value h times faster, accelerating

convergence by reducing error propagation steps, thereby significantly improving numerical stability compared to1-step IQL.

To demonstrate the effectiveness of action chunking in stabilizing training, we train vanilla IQL on the *BallRun* task from the DSRL benchmark (Liu et al., 2023a). As illustrated in Figure 2, vanilla IQL with a chunk length of 1 exhibits slow convergence and unstable Q-values. In contrast, increasing the chunk length leads to faster convergence of the batch-averaged Q-values and smoother training curves, indicating significantly improved stability throughout training.

Action Chunked Penalized Value Function. Our action chunking technique serves as a drop-in modification and can be straightforwardly integrated with IQL. We employ a loss formulation similar to Eq. 12 and 13 to train the h-step penalized reward value function $\overline{Q}_r$ and state value function $\overline{V}_r$:

$$\mathcal{L}_{\overline{Q}_r} = \mathbb{E}_{(s_t, a_{t:t+h}, s_{t+h})\sim D}\Big[\Big(\mathbb{I}(V_c(s_{t+h}) \leq \ell)\Big(\sum_{k=0}^{h-1}\gamma^k r_{t+k} + \gamma^h \overline{V}_r(s_{t+h})\Big) + \mathbb{I}(V_c(s_{t+h}) > \ell)\overline{C} - \overline{Q}_r(s_t, a_{t:t+h})\Big)^2\Big], \tag{15}$$

$$\mathcal{L}_{\overline{V}_r} = \mathbb{E}_{(s_t, a_{t:t+h})\sim D}\Big[L_2^\tau\Big(\overline{Q}_r(s_t, a_{t:t+h}) - \overline{V}_r(s_t)\Big)\Big]. \tag{16}$$

This loss extends the penalized Q-loss to h steps. To ensure consistency, we also train an h-step policy $\pi(a_{t:t+h}|s_t)$ designed to generate a sequence of h consecutive actions. Since maximizing $\overline{Q}_r$ is equivalent to solving a constrained optimization problem, the policy is trained by directly maximizing $\overline{Q}_r$. Analogous to 1-step IQL, we state the following proposition:

Proposition 2 *In the limit as $\tau \to 1$, h-step IQL converges to the optimal value function of an induced MDP where each transition represents h steps in the original MDP.*

Proposition 2 establishes that combining IQL with action chunking is equivalent to learning the optimal value function in an induced MDP. This finding enables the seamless integration of action chunking into our reward-penalty framework, ensuring interpretability. The proof is provided in Appendix A.3.

4.3 Practical Implement

Although the optimal policy maximizes $\overline{V}_r$ to avoid entering unsafe regions, value function approximation errors may still cause the agent to deviate into unsafe states during execution. Once in such states, relying solely on $\overline{V}_r$ provides no mechanism for identifying escape paths back to safety. To overcome this limitation, which is further discussed in Section 5.2, we introduce decoupled objectives for safe and unsafe states. Our approach leverages both$\overline{V}_r$ and the cost value function V_c to guide policy recovery and ensure safety:

$$s \in \mathcal{S}_{\text{safe}} : \max_\pi \mathbb{E}_s\Big[\overline{V}_r^\pi(s)\Big], \qquad s \in \mathcal{S}_{\text{unsafe}} : \max_\pi \mathbb{E}_s\Big[-V_c^\pi(s)\Big]. \tag{17}$$

In the spirit of preserving simplicity and efficiency, we aim for a simple method for policy extraction. We adopt a novel framework based on flow-matching models (Gao et al., 2025; Lipman et al., 2024) utilizing classifier-free guidance (CFG) to generate actions from complex multi-modal distributions (Frans et al., 2025).

We instantiate a single flow-matching network to serve as both the conditional and unconditional policy. The policy is modeled by a velocity field v_θ, conditioned on a partially-noised action $a^i_{t:t+h}$, noise scale i, current state s_t, and an optimality variable $o \in \{\emptyset, 0, 1\}$. The optimality variable is instantiated as follows:

$$\begin{aligned} &s_t \in \mathcal{S}_{\text{safe}}: && s_t \in \mathcal{S}_{\text{unsafe}}: \\ &o = \begin{cases} 1 & \text{if} \quad \overline{A}_r = \overline{Q}_r - \overline{V}_r \geq 0 \\ 0 & \text{if} \quad \overline{A}_r = \overline{Q}_r - \overline{V}_r \leq 0 \end{cases}, && o = \begin{cases} 1 & \text{if} \quad A_c = Q_c - V_c \leq 0 \\ 0 & \text{if} \quad A_c = Q_c - V_c > 0 \end{cases}. \end{aligned} \tag{18}$$

v_θ is trained via the following loss function:

$$\mathcal{L}_v = \mathbb{E}_{(s_t, a_{t:t+h})\sim D}\Big[||v_\theta(a^i_{t:t+h}, i, s_t, o) - (a_{t:t+h} - a^0_{t:t+h})||^2\Big], \tag{19}$$

$$a^i_{t:t+h} = (1-i)a^0_{t:t+h} + i a_{t:t+h}, \tag{20}$$

and where the noise scale i is sampled uniformly from $[0, 1]$, and $a^0_{t:t+h} \sim \mathcal{N}(0, 1)$ is Gaussian noise. When executing, the noised actions are denoised by:

$$\hat{v}^i = v_\theta(a^i_{t:t+h}, i, s_t, \emptyset) + \omega(v_\theta(a^i_{t:t+h}, i, s_t, o) - v_\theta(a^i_{t:t+h}, i, s_t, \emptyset)), \tag{21}$$

where ω is the guidance scale. At each timestep, we generate a sequence of h actions but execute only the first one. Given that most tasks in the DSRL benchmark involve infinite horizons, defining an appropriate safety threshold is challenging. To address this, we adopt the α-quantile of the V_c values from the dataset as the safety threshold. To further enhance safety, we employ rejection sampling (Hatch et al., 2024; Hansen-Estruch et al., 2023; Chen et al., 2023) to select the action with lowest Q_c. Please see Appendix C and Appendix D for more details.

5 Experiments

5.1 Evaluation on DSRL Benchmark

Datasets and Metrics. We evaluate the proposed method on Safety-Gymnasium (Ray et al., 2019) and Bullet-Safety (Gronauer, 2022) tasks within the DSRL benchmark (Liu et al., 2023a), comparing against state-of-the-art safe offline RL algorithms. Performance is measured using normalized return and normalized cost. The normalized return is computed as $R = (R_\pi - R_{\min})/(R_{\max} - R_{\min})$, where R_π is the return of the current policy, and $R_{\max}$ and $R_{\min}$ are the maximum and minimum returns in the dataset. The normalized cost is given by $C = C_\pi/\kappa$, where $\kappa > 0$ is the cost threshold. Following FISOR (Zheng et al., 2024), we treat safety as the primary evaluation criterion and aim to maximize reward only when the safety constraint is satisfied. We set $\kappa = 10$ for Safety-Gymnasium and $\kappa = 5$ for Bullet-Safety tasks, which are used in testing the algorithms aiming to achieve the hard constraints and are hard to achieve in other OSRL algorithms.

Baselines. The baseline algorithms include: i) BC: Behavior cloning; ii) CPQ (Xu et al., 2022): a constrained Q-learning approach that penalizes OOD actions as unsafe; iii) COptiDICE (Lee et al., 2022): a Lagrangian method based on distribution correction estimation (DICE), extending OptiDICE (Lee et al., 2021) for offline safe RL; iv) CDT (Liu et al., 2023b): a Constrained Decision Transformer that infers future costs; v) TREBI (Lin et al., 2023): a cost-budget inference method leveraging the Diffuser (Janner et al., 2022; Ajay et al., 2022) for real-time safe decision-making; vi) FISOR (Zheng et al., 2024): a feasibility guided method combined with diffusion policies.

Main Results. The evaluation results are presented in Table 1. We primarily adopt the evaluation metrics reported in FISOR (Zheng et al., 2024). Our proposed method demonstrates significant performance improvements over all existing baselines. The first five baseline algorithms exhibit substantial constraint violations under strict safety requirements, as a significant gap exists between their theoretical guarantees and practical implementation. Although FISOR explicitly incorporates hard constraints and achieves satisfactory constraint satisfaction, it tends to be overly conservative in many tasks, resulting in comparatively low returns. In contrast, our method maximizes the optimal value function within the safe policy space. Despite employing a more lenient cost metric V_c compared to the feasibility-oriented objective, our approach still satisfies all strict cost constraints. The experimental results clearly demonstrate that our method outperforms all baselines in terms of reward attainment, achieving the highest reward in most of the tasks, while consistently keeping the normalized cost below 1 across all tasks.

5.2 Ablation Study and Analysis

Here we present ablation studies on the key components of our method. Additional ablation results are provided in Appendix E.

Visualization Results. Figure 3 presents a UMAP projection (McInnes et al., 2020) of the value functions V_r, V_c, and $\overline{V}_r$ learned on the ***BallRun*** task, visualized with a subset of $5,000$ randomly sampled states. We observe that states with high V_r values frequently coincide with high V_c values, suggesting that purely maximizing V_r may lead the policy into unsafe states, especially under inaccurate V_c estimates. In contrast, $\overline{V}_r$ assigns low values to states with high V_c, while preserving value trends similar to V_r in other regions, demonstrating the ability of $\overline{V}_r$ to jointly optimize for reward and safety during policy learning.

Table 1: Normalized DSRL (Liu et al., 2023a) benchmark results. ↑ means the higher the better. ↓ means the lower the better. Each value is averaged over 20 evaluation episodes and 3 random seeds. Gray: Unsafe agents. **Bold**: Safe agents whose normalized cost is smaller than 1. **Red**: Safe agents with the highest reward. **Blue**: Safe agents with the second highest reward.

Task	BC		CDT		CPQ		COptiDICE		TREBI		FISOR		ours	
	reward ↑	cost ↓	reward ↑	cost ↓	reward ↑	cost ↓	reward ↑	cost ↓	reward ↑	cost ↓	reward ↑	cost ↓	reward ↑	cost ↓
CarButton1	0.01	6.19	0.17	7.05	0.22	40.06	-0.16	4.63	0.07	3.75	**-0.02**	**0.26**	**0.15**	**0.96**
CarButton2	-0.10	4.47	0.23	12.87	0.08	19.03	-0.17	3.40	**-0.03**	**0.97**	**0.01**	**0.58**	**0.07**	**0.25**
CarPush1	0.21	1.97	0.27	2.12	**0.08**	**0.77**	0.21	1.28	0.26	1.03	**0.28**	**0.28**	**0.29**	**0.36**
CarPush2	0.11	3.89	0.16	4.60	-0.03	10.00	0.10	4.55	0.12	2.65	**0.14**	**0.89**	**0.15**	**0.52**
CarGoal1	0.35	1.54	0.60	3.15	0.33	4.93	0.43	2.81	0.41	1.16	**0.49**	**0.83**	**0.42**	**0.57**
CarGoal2	0.22	3.30	0.45	6.05	0.10	6.31	0.19	2.83	0.13	1.16	**0.06**	**0.33**	**0.32**	**0.67**
AntVel	0.99	12.19	**0.98**	**0.91**	**-1.01**	**0.00**	1.00	10.29	**0.31**	**0.00**	**0.89**	**0.00**	**0.92**	**0.88**
HalfCheetahVel	0.97	17.93	**0.97**	**0.55**	0.08	2.56	**0.43**	**0.00**	**0.87**	**0.23**	**0.89**	**0.00**	**0.95**	**0.13**
SwimmerVel	0.38	2.98	0.67	1.47	0.31	11.58	0.58	23.64	0.42	1.31	**-0.04**	**0.00**	**0.55**	**0.12**
SafetyGym Average	0.35	6.05	0.50	4.31	0.02	10.58	0.29	5.94	0.28	1.36	**0.30**	**0.35**	**0.42**	**0.50**
AntRun	0.73	11.73	0.70	1.88	**0.00**	**0.00**	0.62	3.64	0.63	5.43	**0.45**	**0.03**	**0.62**	**0.53**
BallRun	0.67	11.38	**0.32**	**0.45**	0.85	13.67	0.55	11.32	0.29	4.24	**0.18**	**0.00**	**0.30**	**0.00**
CarRun	0.96	1.88	0.99	1.10	1.06	10.49	**0.92**	**0.00**	0.97	1.01	**0.73**	**0.14**	**0.93**	**0.57**
DroneRun	0.55	5.21	**0.58**	**0.30**	0.02	7.95	0.72	13.77	0.59	1.41	**0.30**	**0.55**	**0.59**	**0.26**
AntCircle	0.65	19.45	0.48	7.44	**0.00**	**0.00**	0.18	13.41	0.37	2.50	**0.20**	**0.00**	**0.32**	**0.23**
BallCircle	0.72	10.02	0.68	2.10	0.40	4.37	0.70	9.06	0.63	1.89	**0.34**	**0.00**	**0.51**	**0.49**
CarCircle	0.65	11.16	0.71	2.19	0.49	4.48	0.44	7.73	**0.49**	**0.73**	**0.40**	**0.11**	**0.52**	**0.11**
DroneCircle	0.82	13.78	0.55	1.29	-0.27	1.29	0.24	2.19	0.54	2.36	**0.48**	**0.00**	**0.52**	**0.32**
BulletGym Average	0.72	10.58	0.63	2.09	0.32	5.28	0.55	7.64	0.56	2.45	**0.39**	**0.10**	**0.54**	**0.31**

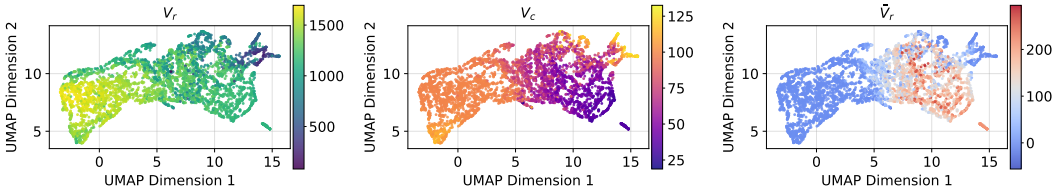

Figure 3: UMAP visualization of V_r, V_c, and $\overline{V}_r$ across 5000 random states in the *BallRun* dataset. Each dot corresponds to a distinct state.

Moreover, we observe that $\overline{V}_r$ assigns nearly identical values to unsafe states, consequently providing insufficient incentive to escape such regions. This observation necessitates a policy designed to actively minimize V_c whenever the agent is in an unsafe state.

Ablation on Safety Threshold. We evaluate the sensitivity of our method to the safety threshold ℓ by testing three different values. The safety thresholds are selected as α-quantile of V_c values in datasets. The results are presented in Figure 4. Since actions that violate the safety constraint lead to termination in an absorbing state, the choice of ℓ directly influences the performance. When $\alpha \leq 0.5$, the normalized score increases steadily with α. For $\alpha > 0.5$, however, performance declines and the normalized cost exhibits oscillations during training, although satisfactory evaluation results can still be achieved using model checkpoints.

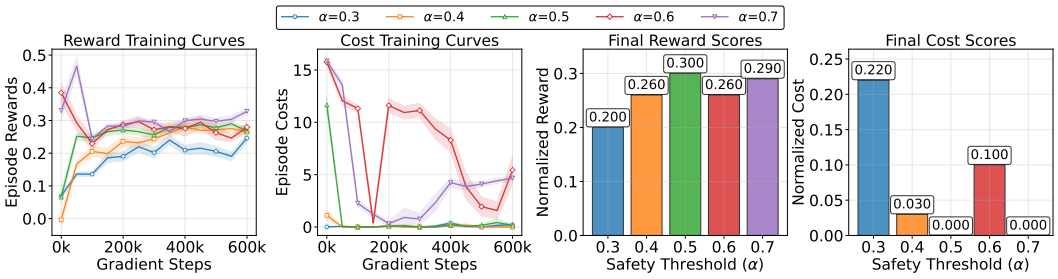

Figure 4: Training curves and normalized scores for different thresholds on the *BallRun* task (Final scores are evaluated over 20 episodes and 3 seeds)

Table 2: Ablation on different design choices. Gray: Unsafe agents. **Bold**: Safe agents whose normalized cost is smaller than 1.

Task	*w/o* $\overline{V}_r$		*w/o* V_c		*AWR actor*		Ours	
	reward ↑	cost ↓	reward ↑	cost ↓	reward ↑	cost ↓	reward ↑	cost ↓
BallRun	0.94	14.69	**0.29**	**0.09**	**0.08**	**0.05**	**0.30**	**0.00**
AntRun	0.62	5.73	0.61	1.16	**0.63**	**0.43**	**0.62**	**0.53**
AntCircle	0.58	13.00	**0.38**	**0.20**	0.34	3.12	**0.32**	**0.23**
DroneRun	0.71	13.28	**0.60**	**0.94**	**0.47**	**0.60**	**0.59**	**0.26**
DroneCircle	0.85	18.5	0.53	1.50	**0.47**	**0.75**	**0.52**	**0.32**
CarGoal1	0.59	1.18	**0.35**	**0.48**	**0.33**	**0.62**	**0.42**	**0.57**
CarGoal2	0.36	2.41	**0.30**	**0.37**	**0.20**	**0.32**	**0.32**	**0.67**

Ablation on Action Chunk Length. To validate the efficacy of action chunking length in value function learning, we conducted ablation studies on *BallRun* and *CarGoal2* tasks. As the different time horizon in Safety-Gymnasium and Bullet-Safety-Gym, we choose $h \in \{1, 3, 5, 7\}$ in *BallRun* and $h \in \{1, 5, 10, 15\}$ in *CarGoal2* for our experiment. As shown in Fig. 5, using values of $h > 1$ leads to consistent performance improvements over the baseline. Specifically, the normalized reward increases steadily with the chunk length h, while the normalized cost decreases.

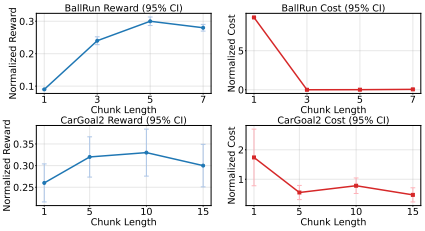

Figure 5: Ablation over chunk length ($h \in \{1, 3, 5, 7\}$) on *BallRun* and ($h \in \{1, 5, 10, 15\}$) on *CarGoal2* tasks.

Ablation on Key Components We evaluate the effectiveness of key components in our method, particularly the region-based reward-penalized value function. To assess the contribution of the penalized value function, we compare against two ablated variants: (1) *w/o* $\overline{V}_r$, which uses the vanilla V_r without safety-aware penalization as the objective of safe states, and (2) *w/o* V_c, which does not incorporate the cost value function V_c for unsafe states. To further demonstrate that our performance is not overly dependent on a specific policy extraction and parameterization approach, we also include an ablation with a three-layer MLP Gaussian actor trained via AWR, denoted as *AWR actor*.

As summarized in Table 2, the variant *w/o* $\overline{V}_r$ exhibits severe constraint violations due to the lack of safety-aware value guidance. *w/o* V_c achieves strong constraint satisfaction in most tasks, but fails in a subset of them as a result of pushing the safety threshold ℓ to its limit in pursuit of higher reward. The *AWR actor* yields constraint satisfaction comparable to our full method but attains lower reward, likely due to the limited expressivity of the parametric policy. In contrast, our complete approach effectively balances constraint satisfaction and reward maximization.

The consistent safety performance of the latter three variants, all of which include the proposed $\overline{V}_r$ function, underscores the effectiveness of our penalized value formulation. Notably, the full constraint satisfaction achieved by the *AWR actor* across all tasks suggests that the safety assurance of our method is robust to the choice of actor architecture.

6 Conclusion

In this work, we propose a novel approach that utilizes IQL to learn safe and high-performing policies from offline dataset. We introduce a penalized reward formulation by integrating cost constraints into reward learning, enabling to approximate the optimal value function within a safe policy space. We employ action chunking to enhance the numerical stability of the training process and mitigate the effect of bootstrap errors, thereby improving the robustness of value function estimation. We provide theoretical analysis, which shows that our penalized value function ensures policy safety. Experiments on DSRL benchmarks demonstrate that our method outperforms existing baseline algorithms in both safety and return, achieving the highest returns in 13 out of 17 tasks while fully satisfying safety constraints.

REFERENCES

Anurag Ajay, Yilun Du, Abhi Gupta, Joshua Tenenbaum, Tommi Jaakkola, and Pulkit Agrawal. Is conditional generative modeling all you need for decision-making? *arXiv preprint arXiv:2211.15657*, 2022.

Eitan Altman. *Constrained Markov decision processes*. Routledge, 2021.

Gaon An, Seungyong Moon, Jang-Hyun Kim, and Hyun Oh Song. Uncertainty-based offline reinforcement learning with diversified q-ensemble. *Advances in neural information processing systems*, 34:7436–7447, 2021.

Per-Arne Andersen, Morten Goodwin, and Ole-Christoffer Granmo. Towards safe reinforcement-learning in industrial grid-warehousing. *Information Sciences*, 537:467–484, 2020.

Aluízio FR Araújo and Arthur PS Braga. Reward-penalty reinforcement learning scheme for planning and reactive behaviour. In *SMC'98 Conference Proceedings. 1998 IEEE International Conference on Systems, Man, and Cybernetics (Cat. No. 98CH36218)*, volume 2, pages 1485–1490. IEEE, 1998.

Somil Bansal, Mo Chen, Sylvia Herbert, and Claire J. Tomlin. Hamilton-jacobi reachability: A brief overview and recent advances. In *2017 IEEE 56th Annual Conference on Decision and Control (CDC)*, pages 2242–2253. IEEE,, 2017.

Homanga Bharadhwaj, Jay Vakil, Mohit Sharma, Abhinav Gupta, Shubham Tulsiani, and Vikash Kumar. Roboagent: Generalization and efficiency in robot manipulation via semantic augmentations and action chunking. In *2024 IEEE International Conference on Robotics and Automation (ICRA)*, pages 4788–4795. IEEE, 2024.

Kevin Black, Manuel Y. Galliker, and Sergey Levine. Real-time execution of action chunking flow policies. *arxiv preprint arxiv:2506.07339*, 2025.

Lukas Brunke, Melissa Greeff, Adam W Hall, Zhaocong Yuan, Siqi Zhou, Jacopo Panerati, and Angela P Schoellig. Safe learning in robotics: From learning-based control to safe reinforcement learning. *Annual Review of Control, Robotics, and Autonomous Systems*, 5(1):411–444, 2022.

Huayu Chen, Cheng Lu, Chengyang Ying, Hang Su, and Jun Zhu. Offline reinforcement learning via high-fidelity generative behavior modeling. *The Eleventh International Conference on Learning Representations*, 2023.

Ricky TQ Chen and Yaron Lipman. Flow matching on general geometries. *arXiv preprint arXiv:2302.03660*, 2023.

Tianyuan Chen, Ronglong Cai, Faguo Wu, and Xiao Zhang. Active: Offline reinforcement learning via adaptive imitation and in-sample v-ensemble. In *The Thirteenth International Conference on Learning Representations*, 2025.

Yinlam Chow, Ofir Nachum, Edgar Duenez-Guzman, and Mohammad Ghavamzadeh. A lyapunov-based approach to safe reinforcement learning. *Advances in Neural Information Processing Systems*, 31, 2018.

Florinel-Alin Croitoru, Vlad Hondru, Radu Tudor Ionescu, and Mubarak Shah. Diffusion models in vision: A survey. *IEEE transactions on pattern analysis and machine intelligence*, 45(9):10850–10869, 2023.

Jaime F Fisac, Neil F Lugovoy, Vicenç Rubies-Royo, Shromona Ghosh, and Claire J Tomlin. Bridging hamilton-jacobi safety analysis and reinforcement learning. In *2019 International Conference on Robotics and Automation (ICRA)*, pages 8550–8556. IEEE, United States, 2019.

Kevin Frans, Seohong Park, Pieter Abbeel, and Sergey Levine. Diffusion guidance is a controllable policy improvement operator. *arxiv preprint arxiv:2505.23458*, 2025.

Scott Fujimoto and Shixiang Shane Gu. A minimalist approach to offline reinforcement learning. *Advances in neural information processing systems*, 34:20132–20145, 2021.

Scott Fujimoto, David Meger, and Doina Precup. Off-policy deep reinforcement learning without exploration. In Kamalika Chaudhuri and Ruslan Salakhutdinov, editors, *Proceedings of the 36th International Conference on Machine Learning*, volume 97 of *PMLR*, pages 2052–2062. PMLR, 09–15 Jun 2019.

Ruiqi Gao, Emiel Hoogeboom, Jonathan Heek, Valentin De Bortoli, Kevin Patrick Murphy, and Tim Salimans. Diffusion models and gaussian flow matching: Two sides of the same coin. *The Fourth Blogpost Track at ICLR 2025*, 2025.

Javier García, Fern, and o Fernández. A comprehensive survey on safe reinforcement learning. *Journal of Machine Learning Research*, 16(1):1437–1480, 2015.

Divyansh Garg, Joey Hejna, Matthieu Geist, and Stefano Ermon. Extreme q-learning: Maxent RL without entropy. *arXiv preprint arXiv:2301.02328*, 2023.

Abraham George and Amir Barati Farimani. One act play: Single demonstration behavior cloning with action chunking transformers. *arXiv preprint arXiv:2309.10175*, 2023.

Sven Gronauer. Bullet-safety-gym: A framework for constrained reinforcement learning. 2022.

Philippe Hansen-Estruch, Ilya Kostrikov, Michael Janner, Jakub Grudzien Kuba, and Sergey Levine. Idql: Implicit q-learning as an actor-critic method with diffusion policies. *arXiv preprint arXiv:2304.10573*, 2023.

Kyle Beltran Hatch, Ashwin Balakrishna, Oier Mees, Suraj Nair, Seohong Park, Blake Wulfe, Masha Itkina, Benjamin Eysenbach, Sergey Levine, Thomas Kollar, and Benjamin Burchfiel. GHIL-glue: Hierarchical control with filtered subgoal images. *CoRL 2024 Workshop on Mastering Robot Manipulation in a World of Abundant Data*, 2024.

Dan Hendrycks and Kevin Gimpel. Gaussian error linear units (gelus). *arxiv preprint arxiv:1606.08415*, 2023.

Matteo Hessel, Joseph Modayil, Hado Van Hasselt, Tom Schaul, Georg Ostrovski, Will Dabney, Dan Horgan, Bilal Piot, Mohammad Azar, and David Silver. Rainbow: Combining improvements in deep reinforcement learning. In *Proceedings of the AAAI conference on artificial intelligence*, volume 32, 2018.

Jonathan Ho and Tim Salimans. Classifier-free diffusion guidance. *NeurIPS 2021 Workshop on Deep Generative Models and Downstream Applications*, 2021.

Jonathan Ho, Ajay Jain, and Pieter Abbeel. Denoising diffusion probabilistic models. *Advances in neural information processing systems*, 33:6840–6851, 2020.

Michael Janner, Yilun Du, Joshua Tenenbaum, and Sergey Levine. Planning with diffusion for flexible behavior synthesis. *arXiv preprint arXiv:2205.09991*, 2022.

Diederik P Kingma and Jimmy Ba. Adam: A method for stochastic optimization. *arXiv preprint arXiv:1412.6980*, 2014.

Prajwal Koirala, Zhanhong Jiang, Soumik Sarkar, and Cody Fleming. Latent safety-constrained policy approach for safe offline reinforcement learning. *arXiv preprint arXiv:2412.08794*, 2025.

Ilya Kostrikov, Ashvin Nair, and Sergey Levine. Offline reinforcement learning with implicit q-learning. *arXiv preprint arXiv:2110.06169*, 2021.

Tadashi Kozuno, Yunhao Tang, Mark Rowland, Rémi Munos, Steven Kapturowski, Will Dabney, Michal Valko, and David Abel. Revisiting peng's q (λ) for modern reinforcement learning. In *International Conference on Machine Learning*, pages 5794–5804. PMLR, 2021.

Aviral Kumar, Justin Fu, Matthew Soh, George Tucker, and Sergey Levine. Stabilizing off-policy q-learning via bootstrapping error reduction. In *Advances in Neural Information Processing Systems*, volume 32. Curran Associates, Inc., 2019.

Aviral Kumar, Aurick Zhou, George Tucker, and Sergey Levine. Conservative q-learning for offline reinforcement learning. *Advances in neural information processing systems*, 33:1179–1191, 2020.

Jongmin Lee, Wonseok Jeon, Byung-Jun Lee, Joelle Pineau, and Kee-Eung Kim. Optidice: Offline policy optimization via stationary distribution correction estimation. *ICML*, pages 6120–6130, 2021.

Jongmin Lee, Cosmin Paduraru, Daniel J Mankowitz, Nicolas Heess, Doina Precup, Kee-Eung Kim, and Arthur Guez. Coptidice: Offline constrained reinforcement learning via stationary distribution correction estimation. *arXiv preprint arXiv:2204.08957*, 2022. doi: 10.48550/arXiv.2204.08957.

Sergey Levine, Aviral Kumar, G. Tucker, and Justin Fu. Offline reinforcement learning: Tutorial, review, and perspectives on open problems. *arXiv preprint arXiv:2005.01643*, 2020.

Qiyang Li, Zhiyuan Zhou, and Sergey Levine. Reinforcement learning with action chunking. *arxiv preprint arxiv:2507.07969*, 2025.

Qian Lin, Bo Tang, Zifan Wu, Chao Yu, Shangqin Mao, Qianlong Xie, Xingxing Wang, and Dong Wang. Safe offline reinforcement learning with real-time budget constraints. In *Proceedings of the 40th International Conference on Machine Learning*, volume 202 of *PMLR*, pages 21127–21152. PMLR, 23–29 Jul 2023.

Yaron Lipman, Ricky TQ Chen, Heli Ben-Hamu, Maximilian Nickel, and Matt Le. Flow matching for generative modeling. *arXiv preprint arXiv:2210.02747*, 2022.

Yaron Lipman, Marton Havasi, Peter Holderrieth, Neta Shaul, Matt Le, Brian Karrer, Ricky T. Q. Chen, David Lopez-Paz, Heli Ben-Hamu, and Itai Gat. Flow matching guide and code. *arxiv preprint arxiv:2412.06264*, 2024.

Yuejiang Liu, Jubayer Ibn Hamid, Annie Xie, Yoonho Lee, Max Du, and Chelsea Finn. Bidirectional decoding: Improving action chunking via guided test-time sampling. *The Thirteenth International Conference on Learning Representations*, 2025.

Zuxin Liu, Zijian Guo, Haohong Lin, Yihang Yao, Jiacheng Zhu, Zhepeng Cen, Hanjiang Hu, Wenhao Yu, Tingnan Zhang, Jie Tan, and Ding Zhao. Datasets and benchmarks for offline safe reinforcement learning. *arXiv preprint arXiv:2306.09303*, 2023a.

Zuxin Liu, Zijian Guo, Yi-Fan Yao, Zhepeng Cen, Wenhao Yu, Tingnan Zhang, and Ding Zhao. Constrained decision transformer for offline safe reinforcement learning. In *International Conference on Machine Learning*, pages 21611–21630. PMLR, 2023b.

Yixiu Mao, Hongchang Zhang, Chen Chen, Yi Xu, and Xiangyang Ji. Supported value regularization for offline reinforcement learning. *Thirty-seventh Conference on Neural Information Processing Systems*, 2023.

Leland McInnes, John Healy, and James Melville. Umap: Uniform manifold approximation and projection for dimension reduction. *arxiv preprint arxiv:1802.03426*, 2020.

Adam Paszke, Sam Gross, Francisco Massa, Adam Lerer, James Bradbury, Gregory Chanan, Trevor Killeen, Zeming Lin, Natalia Gimelshein, Luca Antiga, et al. Pytorch: An imperative style, high-performance deep learning library. *Advances in neural information processing systems*, 32, 2019.

Xue Bin Peng, Aviral Kumar, Grace Zhang, and Sergey Levine. Advantage-weighted regression: Simple and scalable off-policy reinforcement learning. *arXiv preprint arXiv:1910.00177*, 2019.

Alex Ray, Joshua Achiam, and Dario Amodei. Benchmarking safe exploration in deep reinforcement learning. *arXiv preprint arXiv:1910.01708*, 7(1):2, 2019.

Tianyu Shi, Dong Chen, Kaian Chen, and Zhaojian Li. Offline reinforcement learning for autonomous driving with safety and exploration enhancement. *arXiv preprint arXiv:2110.07067*, 2021.

Jascha Sohl-Dickstein, Eric A. Weiss, Niru Maheswaranathan, and Surya Ganguli. Deep unsupervised learning using nonequilibrium thermodynamics. In *Proceedings of the 32nd International Conference on International Conference on Machine Learning - Volume 37*, ICML'15, page 2256–2265. JMLR.org, 2015.

Jiaming Song, Chenlin Meng, and Stefano Ermon. Denoising diffusion implicit models. *arXiv preprint arXiv:2010.02502*, October 2020.

Garrett Thomas, Yuping Luo, and Tengyu Ma. Safe reinforcement learning by imagining the near future. *Advances in Neural Information Processing Systems*, 34:13859–13869, 2021.

Zhendong Wang, Jonathan J Hunt, and Mingyuan Zhou. Diffusion policies as an expressive policy class for offline reinforcement learning. *The Eleventh International Conference on Learning Representations*, 2023.

Zifan Wu, Bo Tang, Qian Lin, Chao Yu, Shangqin Mao, Qianlong Xie, Xingxing Wang, and Dong Wang. Off-policy primal-dual safe reinforcement learning. In *The Twelfth International Conference on Learning Representations*, 2024.

Chenjun Xiao, Han Wang, Yangchen Pan, Adam White, and Martha White. The in-sample softmax for offline reinforcement learning. *The Eleventh International Conference on Learning Representations*, 2023.

Haoran Xu, Xianyuan Zhan, and Xiangyu Zhu. Constraints penalized q-learning for safe offline reinforcement learning. *Proceedings of the AAAI Conference on Artificial Intelligence*, 36(8):8753–8760, 2022.

Haoran Xu, Li Jiang, Jianxiong Li, Zhuoran Yang, Zhaoran Wang, Victor Wai Kin Chan, and Xianyuan Zhan. Offline RL with no OOD actions: In-sample learning via implicit value regularization. *arXiv preprint arXiv:2303.15810*, 2023.

Dongjie Yu, Haitong Ma, Shengbo Li, and Jianyu Chen. Reachability constrained reinforcement learning. In *Proceedings of the 39th International Conference on Machine Learning*, volume 162 of *PMLR*, pages 25636–25655. PMLR, 17–23 Jul 2022.

Qin Zhang, Linrui Zhang, Haoran Xu, Li Shen, Bowen Wang, Yongzhe Chang, Xueqian Wang, Bo Yuan, and Dacheng Tao. Saformer: A conditional sequence modeling approach to offline safe reinforcement learning. *arXiv preprint arXiv:2301.12203*, 2023.

Yinan Zheng, Jianxiong Li, Dongjie Yu, Yujie Yang, Shengbo Eben Li, Xianyuan Zhan, and Jingjing Liu. Safe offline reinforcement learning with feasibility-guided diffusion model. In *The Twelfth International Conference on Learning Representations*, 2024.

A Theoretical Interpretations

A.1 Proof to Proposition 1

proof. Let V_{-C}^{π} denotes the cost value function in reward penalty MDP $\mathcal{M}_C$, is defined as

$$V_{-C}^{\pi}(s) = \mathbb{E}_{s_0=s, a_t\sim\pi, s_t\sim P_{-C}}\Big[\sum_{t=0}^{T-1}\gamma^t \mathbb{I}(s_t = s_a)(-C)\Big], \tag{22}$$

where P_{-C} is the transition dynamic of $\mathcal{M}_C$.

Consider an unsafe policy π_1 in the original MDP $\mathcal{M}$, such that $V_c^{\pi_1}(\rho_0) \geq \ell$, and assume the cost function $c \in \{0, 1\}$. Then in $\mathcal{M}_C$, we have $V_{-C}^{\pi_1}(\rho_0) \leq -C\ell$, since the absorbing nature of $\mathcal{M}_C$ leads to a higher visitation frequency of unsafe states under π_1 compared to $\mathcal{M}$. Then,

$$\begin{aligned}
\overline{V}_r^{\pi_1}(\rho_0) &= \mathbb{E}_{s_0\sim\rho_0, a_t\sim\pi_1, s_t\sim P_{-C}}\Big[\sum_{t=0}^{T-1}\gamma^t \overline{r}_t\Big] \\
&= \mathbb{E}_{s_0\sim\rho_0, a_t\sim\pi_1, s_t\sim P_{-C}}\Big[\sum_{t=0}^{T-1}\gamma^t (\mathbb{I}(s_t \neq s_a) r_t + \mathbb{I}(s_t = s_a)(-C))\Big] \\
&= \mathbb{E}_{s_0\sim\rho_0, a_t\sim\pi_1, s_t\sim P_{-C}}\Big[\sum_{t=0}^{T-1}\gamma^t (\mathbb{I}(s_t \neq s_a) r_t\Big] \\
&\quad + \mathbb{E}_{s_0\sim\rho_0, a_t\sim\pi_1, s_t\sim P_{-C}}\Big[\sum_{t=0}^{T-1}\gamma^t \mathbb{I}(s_t = s_a)(-C))\Big] \\
&\leq \mathbb{E}_{s_0\sim\rho_0, a_t\sim\pi_1, s_t\sim P}\Big[\sum_{t=0}^{T-1}\gamma^t r_t\Big] + \mathbb{E}_{s_0\sim\rho_0, a_t\sim\pi_1, s_t\sim P_{-C}}\Big[\sum_{t=0}^{T-1}\gamma^t (\mathbb{I}(s_t = s_a)(-C))\Big] \\
&= V_r^{\pi_1}(\rho_0) + V_{-C}^{\pi_1}(\rho_0) \\
&\leq V_r^{\pi_1}(\rho_0) - C\ell \\
&\leq \sum_{t=0}^{T-1}\gamma^t r_{\max} - C\ell.
\end{aligned} \tag{23}$$

Now, assume that for any $\ell \geq 0$, there exists at least one safe policy π_2 such that $V_c^{\pi_2}(\rho_0) \leq l$. Setting $\ell = 0$, π_2 never enters s_a, and thus the minimum reward it receives in $\mathcal{M}_c$ is $\sum_{t=0}^{T-1}\gamma^t r_{\min}$. To ensure that π_1 is suboptimal, it suffices to choose C such that:

$$\sum_{t=0}^{T-1}\gamma^t r_{\max} - C\ell < \sum_{t=0}^{T-1}\gamma^t r_{\min}. \tag{24}$$

Rearranging, we derive

$$C > \frac{\sum_{t=0}^{T-1}\gamma^t (r_{\max} - r_{\min})}{\ell}. \tag{25}$$

For the infinite-horizon case where $T = \infty$, this simplifies to

$$C > \frac{r_{\max} - r_{\min}}{(1-\gamma)\ell}. \tag{26}$$

A.2 Discussion of Optimality

In this section, we will show that when $C \to \infty$, the optimal policy in the penalized MDP $\mathcal{M}_C$ is also the optimal policy in the original MDP $\mathcal{M}$ with $\ell = 0$.

Let π_C^* denote the optimal solution to $\mathcal{M}_C$, and π^* denote the optimal solution to $\mathcal{M}$. When $l = 0$, $V_c^{\pi^*}(\rho_0) = 0$. Therefore, π^* will never enter the unsafe region (i.e., all states with state visitation distribution $d^{\pi^*} > 0$ have zero cost). In $\mathcal{M}_C$, π^* will never receive the $-C$ penalty.

As $C \to \infty$, π_C^* will also never receive the $-C$ reward, since there exists at least one policy (e.g., π^*) whose value is greater than $\sum_{t=0}^{T-1} \gamma^t r_{\min}$. Hence, the state visitation distribution of π_C^* in $\mathcal{M}_C$ is zero over the absorbing state s_a. Excluding s_a, the transition structure of $\mathcal{M}_C$ is identical to that of $\mathcal{M}$. Therefore, π_C^* is also the optimal policy for $\mathcal{M}$.

A.3 Proof to Proposition 2

proof. For a MDP $\mathcal{M}$, we define a new MDP $\mathcal{M}_h$. M_h has the same state space $\mathcal{S}$ as $\mathcal{M}$. The new action space $\mathcal{A}_h$, the h-step reward function r_h, and transition probabilities P_h is:

$$\mathcal{A}_h = \underbrace{\mathcal{A} \times \mathcal{A} \times \cdots \mathcal{A}}_{h \text{ times}}, \tag{27}$$

$$r_h(s_t, a_{t:t+h}) = \sum_{k=0}^{h-1} \gamma^k r_{t+k}, \tag{28}$$

$$P_h(s_{t+h}|s_t, a_t) = \sum_{s_{t+1}, \cdots, s_{t+h-1}} \prod_{k=t}^{t+h-1} P(s_{k+1}|s_k, a_k). \tag{29}$$

Then we consider the offline setting, where data are collected by a behavior policy $\mu(a_{t:t+h}|s_t)$. Following Theorem 3 of Kostrikov et al. (2021), we have

$$\lim_{\tau \to 1} V_\tau(s_t) = \max_{\substack{a_{t:t+h} \in \mathcal{A}_h \\ \text{s.t. } \mu(a_{t:t+h}|s_t) > 0}} Q^*(s_t, a_{t:t+h}). \tag{30}$$

The above discussion says that IQL with action chunking still approximates an optimal value function in $\mathcal{M}_h$. While the optimal action for each state is a chunk of actions in the dataset. We further extend the h-step IQL to obtain the explicit form of the corresponding implicit policy. Following Theorem 4.1 of Hansen-Estruch et al. (2023), we write the objective as

$$\arg\min_{V(s_t)} \mathbb{E}_{a_{t:t+h} \sim \mu}[f(Q(s_t, a_{t:t+h}) - V(s_t))],$$

where f is arbitrary convex function, and $f = L^\tau$ in IQL. Note that the objective function is convex with respect to $V(s)$

$$\begin{aligned} 0 &= \frac{\partial}{\partial V(s)} \mathbb{E}_{a_{t:t+h} \sim \mu}[f(Q(s_t, a_{t:t+h}) - V(s_t))]\Big|_{V=V^*} \\ &= -\mathbb{E}_{a_{t:t+h} \sim \mu}[f'(Q(s_t, a_{t:t+h}) - V^*(s_t))] \\ &= \mathbb{E}_{a_{t:t+h} \sim \mu}\left[\frac{|f'(Q(s_t, a_{t:t+h}) - V^*(s_t))|(Q(s_t, a_{t:t+h}) - V^*(s_t))}{|Q(s_t, a_{t:t+h}) - V^*(s_t)|}\right]. \end{aligned} \tag{31}$$

We then define the implicit policy to be

$$\pi_{\text{imp}}(a_{t:t+h}|s_t) = \frac{\mu(a_{t:t+h}|s_t)|f'(Q(s_t, a_{t:t+h}) - V^*(s_t))|}{Z_{\text{imp}}|Q(s_t, a_{t:t+h}) - V^*(s_t)|}, \tag{32}$$

where Z_{imp} is a normalization constant, and rewrite the above expression as

$$\begin{aligned} &= \mathbb{E}_{a_{t:t+h} \sim \pi_{\text{imp}}}[(Q(s_t, a_{t:t+h}) - V^*(s_t))] \\ &= \frac{\partial}{\partial V(s_t)} - \frac{1}{2} \cdot \mathbb{E}_{a \sim \pi_{\text{imp}}}[(Q(s_t, a_{t:t+h}) - V(s_t))^2]\Big|_{V=V^*} = 0. \end{aligned} \tag{33}$$

With the above discussion, we obtain the action chunking policy is also a reweighted form of behavior policy like 1-step IQL do. For loss in Eq. 15, we have that the implicit policy is

$$\pi_{\text{imp}}(a_{t:t+h}|s_t) \propto \frac{\mu(a_{t:t+h}|s_t)|f'(\overline{Q}(s_t, a_{t:t+h}) - \overline{V}^*(s_t))|}{|\overline{Q}(s_t, a_{t:t+h}) - \overline{V}^*(s_t)|}. \tag{34}$$

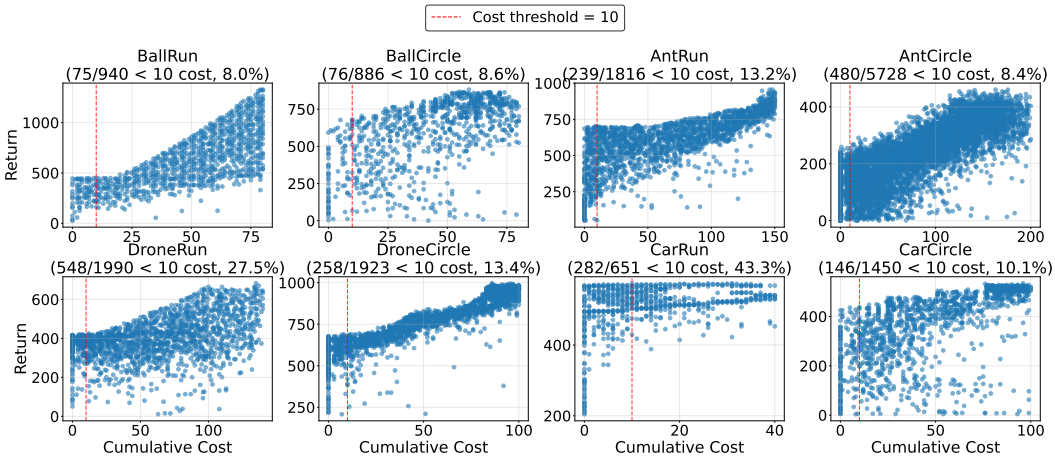

Figure 6: Dataset Composition Overview for Bullet-Safety-Gym Tasks.

B Benchmark Details

B.1 Safety Gymnasium

Safety-Gymnasium (Ray et al., 2019), a MuJoCo-based benchmark for safe RL, evaluates the trade-off between performance and safety through two categories of environments. The first involves obstacle avoidance tasks performed by a *Car* agent across three scenarios (*Goal*, *Button*, and *Push*), each with two difficulty levels (1 and 2). These tasks represent an important class of real-world reinforcement learning problems in which an agent must move through an environment and interact with objects to achieve a goal. The agent receives rewards for task completion and penalties for contacting hazards. These environments are named in the format $\{Agent\}\{Task\}\{Difficulty\}$ (e.g., *CarGoal1*). The second category consists of velocity-constrained environments featuring three agents (*Ant*, *HalfCheetah*, and *Swimmer*), where the objective is to maximize forward movement reward while adhering to safe speed limits. This tests the ability to balance performance with precise control to avoid failures due to overspeed. Environments in this category follow the naming scheme AgentVel (e.g., *AntVelocity*).

B.2 Bullet Safey Gym

Bullet-Safety-Gym (Gronauer, 2022) is a safe RL benchmark based on the PyBullet engine. Unlike Safety-Gymnasium, it uses shorter time horizons to enable faster training, serving as its efficient complementary alternative, with a broader variety of robotic agents, including *Ball*, *Car*, *Drone*, and *Ant*. The task settings remain relatively straightforward, offering two main types: *Circle* and *Run*. Each environment is named concisely using the convention $\{Agent\}\{Task\}$, (e.g., *AntCircle*).

B.3 Composition of the Dataset

The datasets used in our evaluations predominantly contain a mix of safe and unsafe trajectories. The safety compliance of policies during evaluation is determined by their adherence to the undiscounted cost-return threshold. We provide further details regarding the dataset composition.

Figure 6 and Figure 7 show the reward and cost returns of trajectories in the dataset, with each point representing one pre-collected trajectory. Most datasets used in our evaluation contain both safe and unsafe trajectories. The cost limit is indicated by a red dashed line for reference. A significant number of trajectories exceed this limit, and unsafe trajectories often outnumber safe ones.

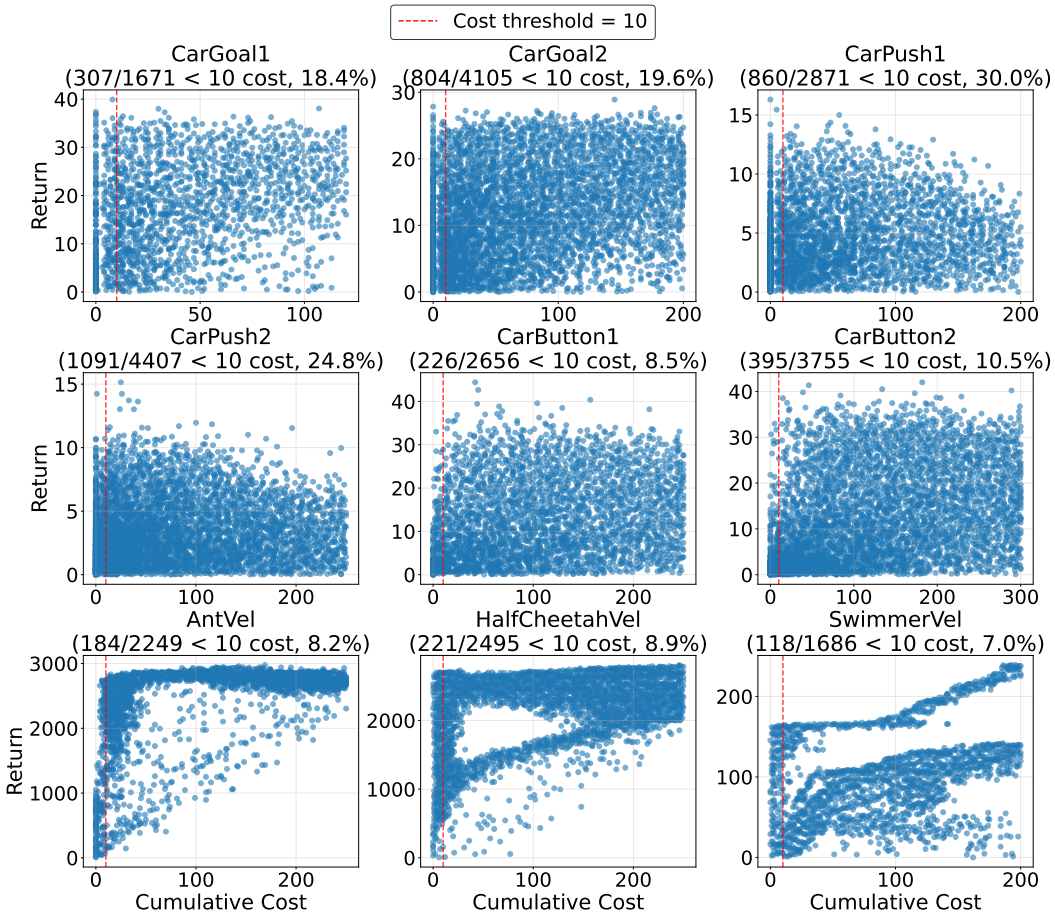

Figure 7: Dataset Composition Overview for Safety-Gymnasium Tasks.

Algorithm 1 CFG Training

for Each gradient steps **do**
  $(s, a) \sim D$, $a_0 \sim \mathcal{N}(0, I)$, $t \sim U(0, 1)$
  Label with optimality $o \in \{0, 1\}$.
  If $\text{rand}() < 0.1$, set optimality $o = \emptyset$.
  $a_t \leftarrow (1 - t)\, a_0 + t\, a$
  $\theta \leftarrow \nabla_\theta \| v_\theta(a_t, t, s, o) - (a - a_0) \|^2$
end for

Algorithm 2 CFG Sampling

$a \sim \mathcal{N}(0, I)$
$t \leftarrow 0$
for $n \in [0, \ldots, N-1]$ **do**
  $v = (1 - w)\, v_\theta(a, t, s, \emptyset) + w\, v_\theta(a, t, s, o = 1)$
  $a \leftarrow a + (n/N)v$
  $t \leftarrow t + (n/N)$
end for
return a

C Flow Matching and Classifier Free Guidance

Flow Matching. Flow matching is an expressive diffusion-style generative model that enjoys simplicity compared to denoising diffusions. Given a data distribution $p(x) \in \Delta(\mathbb{R}^d)$ on a d-dimensional Euclidean space, flow matching aims to construct a time-dependent vector field $v_\theta : [0, 1] \times \mathbb{R}^d \to \mathbb{R}^d$ such that a flow $\phi : [0, 1] \times \mathbb{R}^d \to \mathbb{R}^d$ is described by:

$$\frac{d}{dt}\phi_t(x) = v_\theta(\phi_t(x)), \tag{35}$$

where $\phi_1(x) = x$. A simplest variant of flow matching is based on linear paths and uniform time sampling, and trained by minimizing the following loss:

$$\mathbb{E}_{x^0 \sim \mathcal{N}(0, I_d), x^1 \sim p(x), t \sim \text{Unif}[0,1]} \Big[\| v_\theta(t, x^t) - (x^1 - x^0) \|^2 \Big], \tag{36}$$

where $\mathcal{N}(0, I_d)$ is the d-dimensional standard normal distribution, $\text{Unif}[0, 1]$ denotes the uniform distribution, and $x^t = (1 - t)x^0 + tx^t$.

Classifier Free Guidance. Classifier-free guidance (CFG) (Ho and Salimans, 2021) uses Bayes' rule to guide the generated distribution to the desired direction. CFG trains a single diffusion model to implement both conditional and unconditional ones. Rather than sampling in the direction of a trained classifier's gradient, the CFG approach derives the guided distribution through the following formula:

$$\nabla_x \log q(x) = \nabla_x \log p(x) + \omega(\nabla_x \log p(x|y) - \nabla_x \log p(x)), \tag{37}$$

where $q(x)$ is the guided distribution.

Policy Improvement by CFG. In recent work, Frans et al. (2025) proposed the use of CFG to steer a diffusion policy toward optimality, demonstrating strong empirical performance. The authors parameterize policies as a product of two components: a reference policy $\hat{\pi}$ and an optimality function $f : \mathbb{R} \to \mathbb{R}$. The policy is defined as follows:

$$\pi(a|s) \propto \hat{\pi}(a|s) \cdot f\big(A(s, a)\big), \tag{38}$$

where $A(s, a)$ denotes the advantage function. It is shown that if f is non-negative and monotonically increasing with respect to A, then π is guaranteed to improve upon $\hat{\pi}$. This result can be generalized to an exponentiated form:

$$\pi(a|s) \propto \hat{\pi}(a|s) \cdot f\big(A(s, a)\big)^\omega, \tag{39}$$

where ω controls the degree of improvement.

In practice, the optimality function f is cast as a binary random variable $o \in \{\emptyset, 0, 1\}$, with a likelihood proportional to f: $p(o|s, a) \propto f(A(s, a))$. A flow-matching instantiation of this framework is detailed in Algorithm 1 and Algorithm 2.

D Implement Details

Our implementation is based on PyTorch (Paszke et al., 2019). All experiments were conducted on a single NVIDIA RTX 4090 GPU, with each run completed within 4 hours. Further implementation details are provided in the following section.

D.1 PSEUDOCODE

To provide an intuitive understanding of our method, we present a brief summary of it in this subsection.

Algorithm 3 R2PAC

```
Initialize parameters Q̄_r, Q_c, V̄_r, V_c, v_θ
Value function learning (h-step IQL):
for each gradient steps do
    get batch of (s_t, a_{t:t+h}, s_{t+h}) ~ D
    update Q̄_r , Q_c, V̄_r and V_c by the Eq. 15 and Eq. 16
    update target networks
end for
Policy extraction (CFG):
for each gradient steps do
    get batch of (s_t, a_{t:t+h}) ~ D
    update vector filed v_θ using Eq. 19
end for
```

Through the action chunking technique, action sequences are employed as inputs to the Q-function during training. We extend the 1-step approach employed in IQL to incorporate h consecutive actions. Specifically, we utilize transitions of the form $(s_t, a_{t:t+h}, s_{t+h})$, and apply expectile regression, using the same state-value function estimation method as IQL, to approximate the optimal value function. For $\mathcal{L}_{Q_r}$, the loss calculation includes an additional penalty term for safety constraint violations, as defined in Eq. 7.

Our policy extraction is performed using h-step value functions. We employ a CFG method for policy extraction, based on Frans et al. (2025), with slight adjustments to the optimality criteria. Our actor is designed to generate a sequence of h consecutive actions. During execution, however, only the first action in each sequence is executed, consistent with standard 1-step actors.

D.2 HYPERPARAMETER

To facilitate understanding and analysis of hyperparameter effects, we categorize them into two classes: unified hyperparameters for all DSRL experiments (Table 3) and per-task hyperparameters (Table 4).

To achieve optimal performance across tasks, we carefully tuned our algorithm's key hyperparameters. The hyperparameter configurations are provided in Table 3. The CFG scale ω balances task performance against behavioral regularization: a higher ω prioritizes high-value actions, while a lower ω adheres more closely to the behavior policy. These selections reflect inherent task requirements. In our experiments, we found that a mild guidance scale ($\omega = 2.0$) consistently achieved high performance, and was therefore kept fixed across all tasks.

The cost threshold ℓ, which serves as a metric to separate safe and unsafe regions, significantly influences performance. A high value of ℓ may cause the policy to overlook safety constraints, whereas a low value can overly constrain the policy, hindering reward maximization. Fine-tuning ℓ is a challenging and labor-intensive process. To reduce the workload, we propose a principled approach that sets ℓ as the α-quantile of the dataset value. As illustrated in Figure 6, datasets vary in their composition of safe and unsafe trajectories. Empirically, we observe that datasets with a higher proportion of safe trajectories tolerate a larger ℓ, leading to improved performance without constraint violation. Conversely, for datasets with fewer safe trajectories, a smaller ℓ is preferable. Accordingly, we adaptively set ℓ as the α-quantile of the state value V_c during training. This approach eliminates the need for manual tuning of ℓ and thus yields robust and high-performing results in our experiments.

Another important hyperparameter is the penalty coefficient $\overline{C}$. Theoretically, setting $\overline{C}$ as large as possible is preferred. However, in practice, an excessively large $\overline{C}$ may hinder value function approximation due to limited model capacity. Empirically, we observe that our method is relatively

Table 3: Hyperparameters for DSRL experiments.

Hyperparameter	**Value**
Learning rate	0.0003
Optimizer	Adam (Kingma and Ba, 2014)
Gradient steps	600000
Minibatch size	1024
MLP dimensions	$[512, 512, 512, 512]$
Nonlinearity	GELU (Hendrycks and Gimpel, 2023)
Flow steps	32
Flow time sampling distribution	$\mathrm{Unif}([0, 1])$
CFG scale w	2.0
Generated candidate numbers	16
Chunk length h	1 for *HalfCheetahVel* task and 5 for others
Expectile τ	0.9
Discount factor γ	0.99
Target critic soft update	0.005
Reward scale	200.0 for *Car* series task in Safey-Gymnasium, 1.0 for others
Cost scale	1.0

Table 4: Per-task hyperparameters selection

Task	**Quantile α**	**Penalty Coefficient $\overline{C}$**
`AntRun`	0.7	1.0
`BallRun`	0.5	1.0
`CarRun`	0.95	1.0
`DroneRun`	0.7	1.0
`AntCircle`	0.7	1.0
`BallCircle`	0.85	1.0
`CarCircle`	0.9	1.0
`DroneCircle`	0.7	1.0
`CarPush1`	0.9	10.0
`CarPush2`	0.9	10.0
`CarGoal1`	0.9	10.0
`CarGoal2`	0.9	10.0
`CarButton1`	0.8	10.0
`CarButton2`	0.5	10.0
`AntVelocity`	0.95	1.0
`HalfCheetahVelocity`	0.99	1.0
`SwimmerVelocity`	0.7	1.0

insensitive to the choice of $\overline{C}$. Therefore, we offer only two options for $\overline{C}$, as shown in Table 4, to simplify hyperparameter tuning.

E Additional Experimental Results

E.1 Additional Visualization Results

We provide more UMAP visualization over V_r, V_c, and $\overline{V}_r$ to elucidate the advantage of our method in Figure.8.

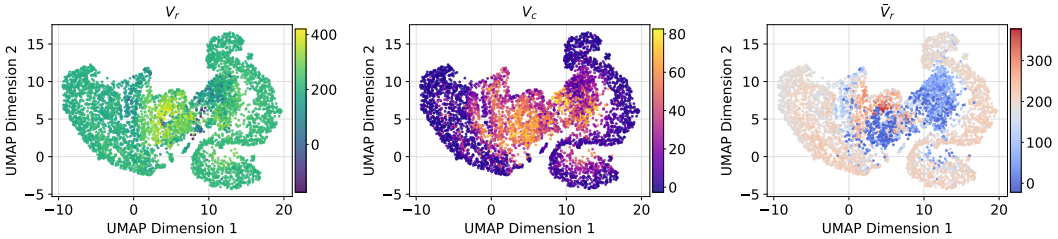

(a) UMAP visualization in the *DroneRun* task.

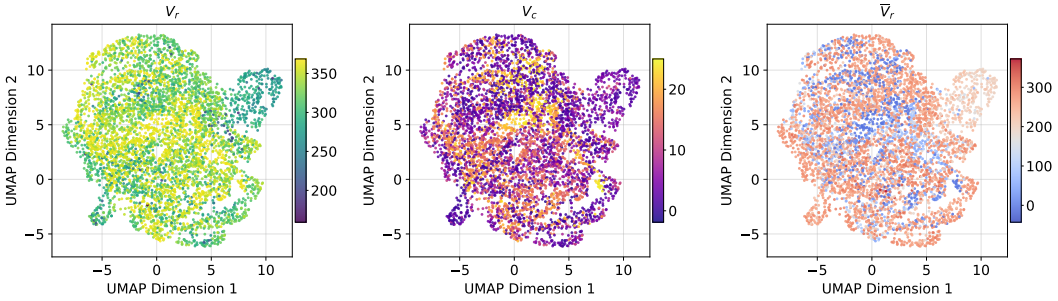

(b) UMAP visualization in the *DroneCircle* task.

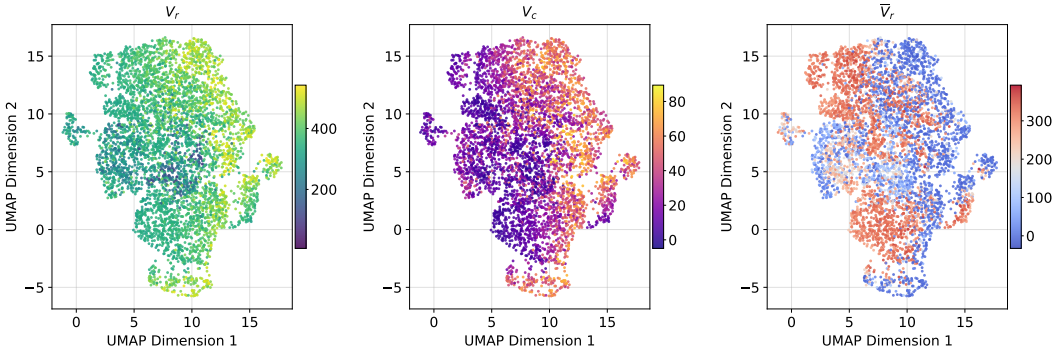

(c) UMAP visualization in the *AntRun* task.

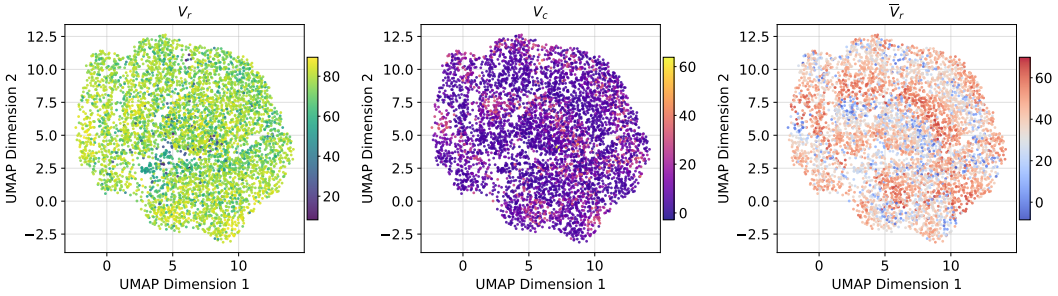

(d) UMAP visualization in the *AntCircle* task.

Figure 8: Comparative visualization of learned state representations using UMAP dimensionality reduction across four distinct locomotion tasks: *DroneRun*, *DroneCircle*, *AntRun*, and *AntCircle*.

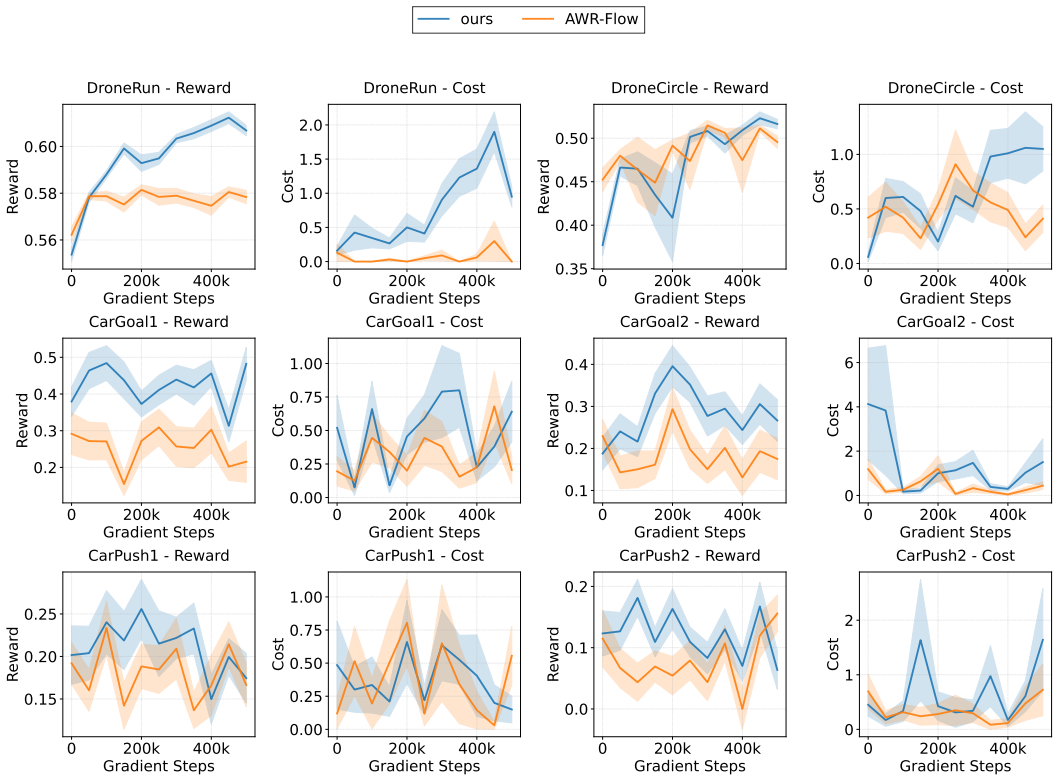

Figure 9: Training curves of our method and *AWR-Flow* on *DroneRun*, *DroneCircle*, *CarGoal1*, *CarGoal2*, *CarPush1*, and *CarPush2* tasks

E.2 Additional Ablation on Policy Extraction Choice

We demonstrate that the h-step penalized reward value function is the most effective component of our method. To verify the irrelevance of the policy extraction manner, we compare the CFG actor with the AWR actor.

In Section 5, we have conducted the ablation studies using a three-layer MLP Gaussian actor, which is trained by

$$\mathcal{L}_\pi = \mathbb{E}_{(s,a)\sim D}\Big[\Big(\mathbb{I}_{s\in\mathcal{S}_{\text{safe}}}\exp(\alpha(\overline{Q}_r - \overline{V}_r) + \mathbb{I}_{s\in\mathcal{S}_{\text{safe}}}\exp(\beta(V_c - Q_c)\Big)\log\pi_\phi(a|s)\Big], \tag{40}$$

where $\alpha, \beta > 0$ denote the temperature parameter. In our experiment, we set both α and β as 6.0.

To isolate the effect of the policy parameterization method, we also do an extra experiment using the flow-matching framework for the AWR actor. We denote it as *AWR-Flow*. The loss function is defined as:

$$\begin{aligned}\mathcal{L}_v =& \mathbb{E}_{(s_t,a_{t:t+h})\sim D}\Big[\Big(\mathbb{I}_{s\in\mathcal{S}_{\text{safe}}}\exp(\alpha(\overline{Q}_r - \overline{V}_r) \\ &+ \mathbb{I}_{s\in\mathcal{S}_{\text{safe}}}\exp(\beta(V_c - Q_c)\Big)||v_\theta(a^i_{t:t+h}, i, s_t) - (a_{t:t+h} - a^0_{t:t+h})||^2\Big].\end{aligned} \tag{41}$$

As shown in Figure 9, both *AWR-Flow* and our CFG method demonstrate enhanced safety assurance and achieve higher final rewards in most tasks by maximizing $\overline{V}_r$.

E.3 Cost Metric Choice

Our method can be readily adapted to different safety metrics. A particularly promising metric called feasibility (Zheng et al., 2024; Yu et al., 2022; Bansal et al., 2017) has recently been introduced in RL, which is Hamilton–Jacobi (HJ) reachability, notable for its hard constraint guarantees and

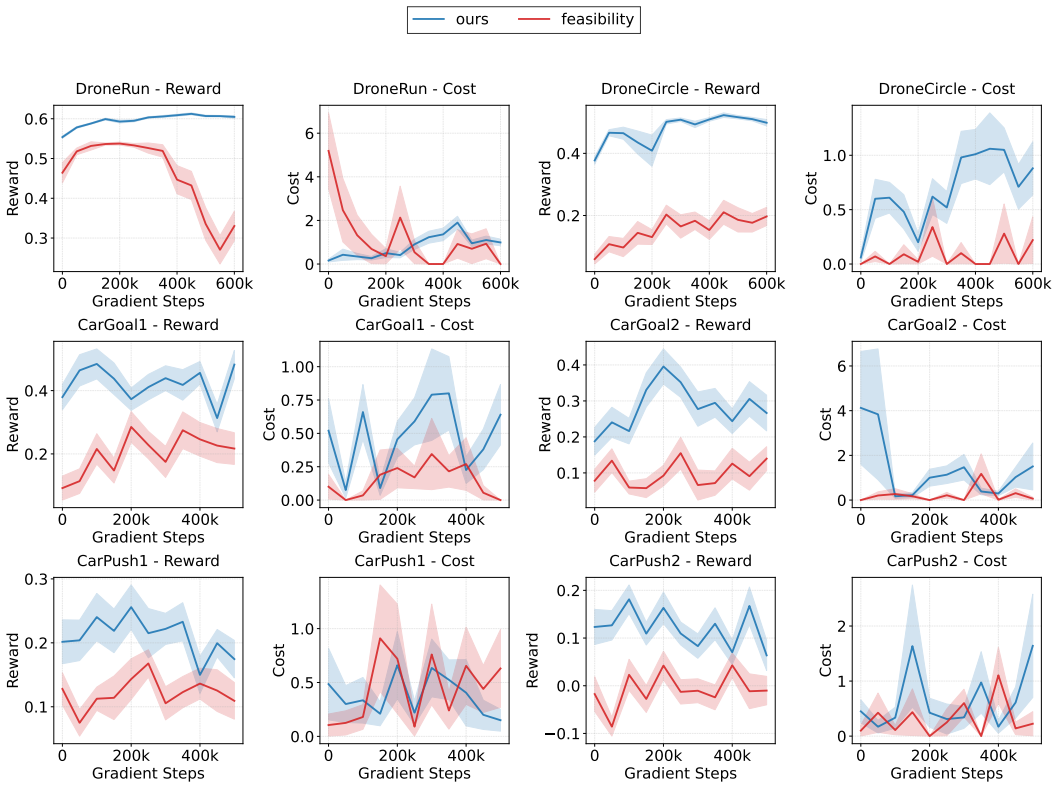

Figure 10: Training curves of our method and *feasibility* on *DroneRun*, *DroneCircle*, *CarGoal1*, *CarGoal2*, *CarPush1*, and *CarPush2* tasks

Bellman backup-style updating. The feasibility Q-function is updated as

$$Q_h(s,a) \leftarrow (1-\gamma)h(s) + \gamma \max\{h(s), V_h(s')\}, \tag{42}$$

where h is the state constraint function.

We evaluate a variant of our method, denoted as *feasibility*, wherein HJ reachability is adopted as the criterion for distinguishing safe and unsafe regions while keeping all other components unchanged. As shown in Figure 10, this variant maintains a plausible constraint-satisfaction capability. We note a slight performance drop, which we attribute to the strict, hard-constraint nature of the HJ reachability condition.

F Training Curve

We evaluate our method on 17 tasks from the DSRL benchmark. The training curves are presented in Figure 11 and Figure 12. All experiments use the same hyperparameters specified in Table 3 and Table 4.

G Limitations

One limitation of our current study stems from the need to fine-tune the safety threshold l across different datasets, which is particularly challenging due to varying proportions of unsafe transitions. To mitigate this issue, we introduce a simple adaptive thresholding method based on the α-quantile. Looking forward, we plan to develop more resilient cost metrics that are robust to uncertain or unsafe data distributions, such as feasibility analysis.

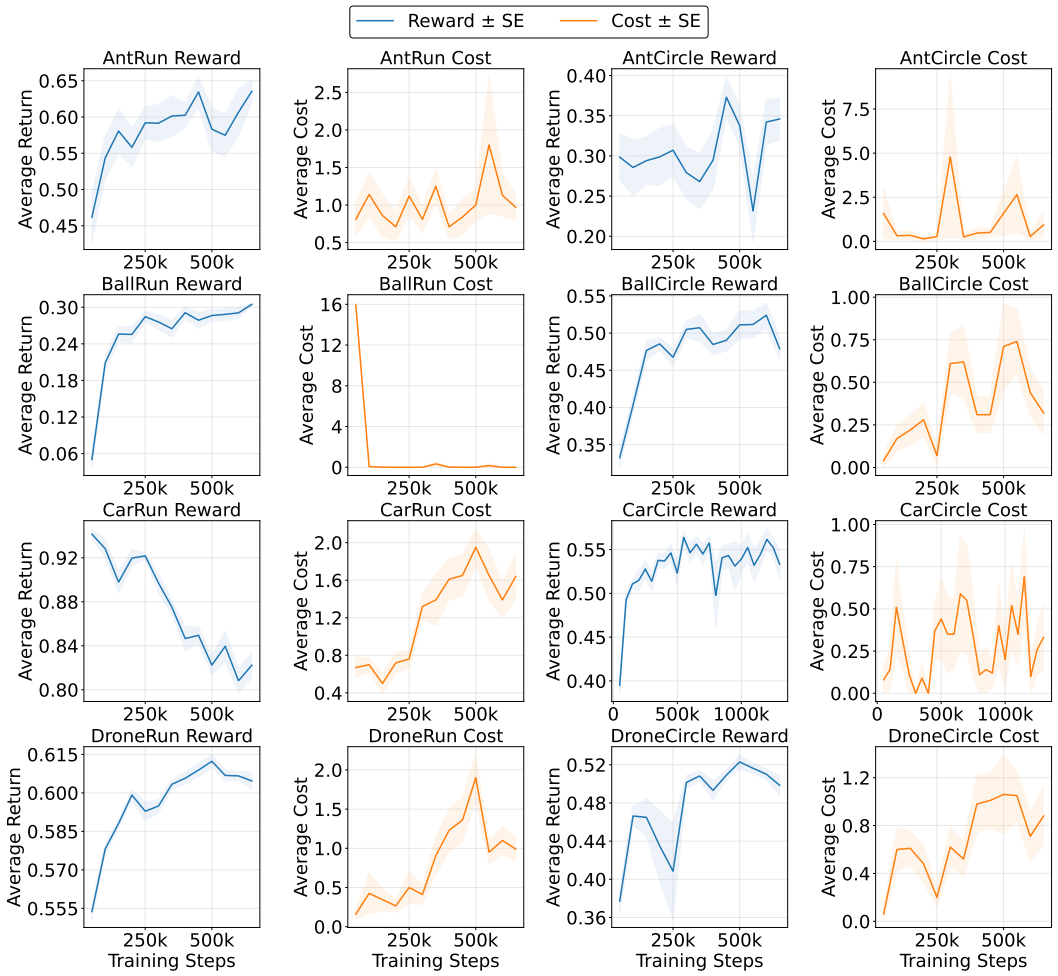

Figure 11: Training curves on the Bullet-Safety-Gym tasks.

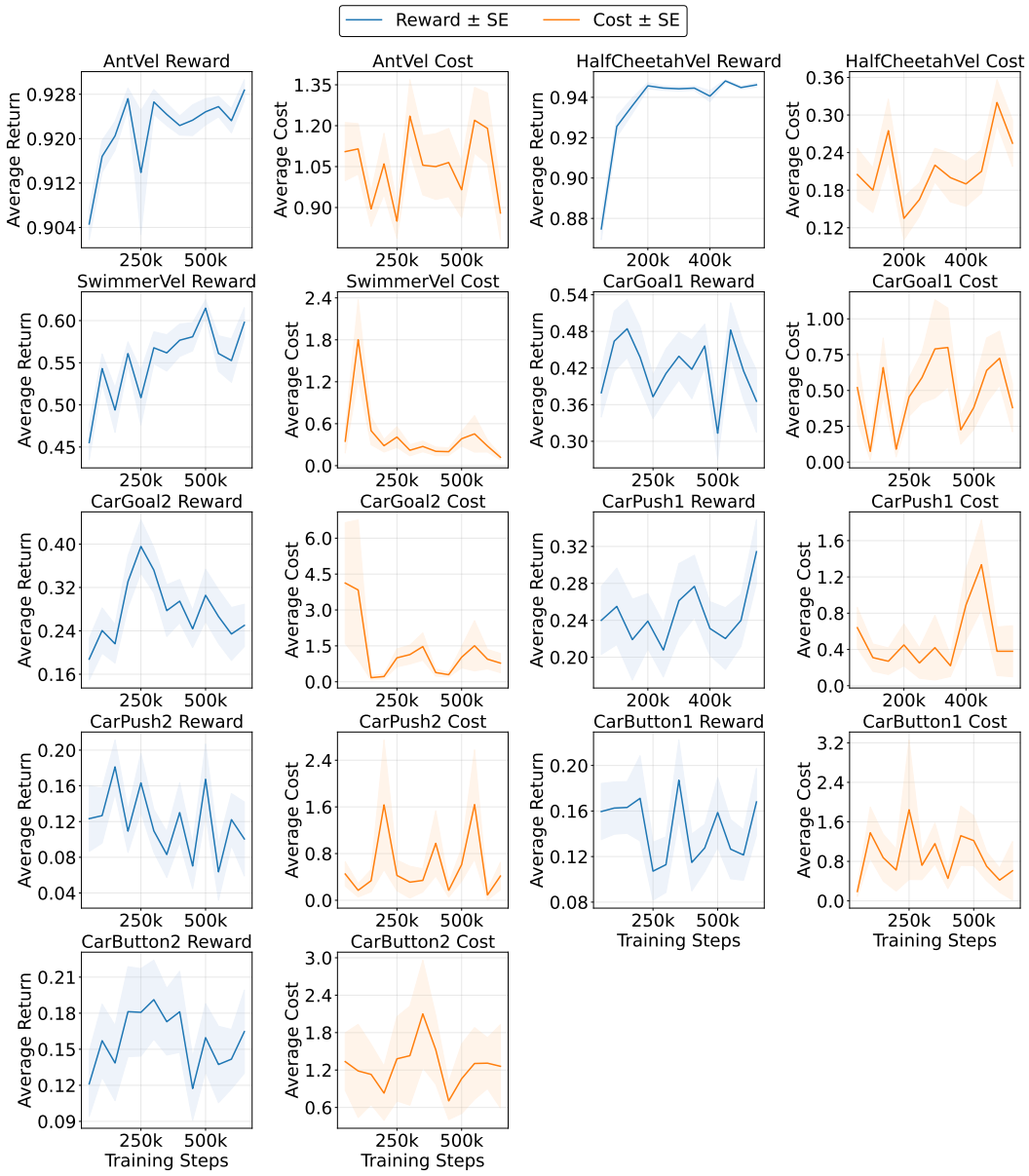

Figure 12: Training curves on the Safety-Gymnasium tasks.